# Comparing a Few Qubit Systems for Superconducting Hardware Compatibility and Circuit Design Sensitivity in Qiskit

Hillol Biswas,

Department of Electrical and Computer Engineering,
Democritus University of Thrace, Xanthi, GREECE
hillbisw@ee.duth.gr

Abstract— In the current quantum computing ecosystem, building complex and integrated circuits for addressing real-world problems often involves using basic historical components like Bell states to take advantage of superposition, entanglement, and coherence. The availability of the simulator and the IBM quantum computing endeavor through Qiskit further broadens the scope of application based on domain use. In the NISQ era, however, error mitigation is a criterion that is applied when comparing a QPU run result with the simulator. As the real-world scope of application for quantum computing is being broadened, using simulators as a baseline offers confidence; however, concerns about computation resources and availability arise in the high-speed computational regime. As complex problems entail using a larger number of superconducting physical qubits, what should be the basis of framing a quantum circuit for building quantum algorithms in a real-world scenario, given hardware compatibility that should ideally provide confidence baselining with the simulator outcome? This work implements three base circuits for different qubit systems in the simulator and corresponding 127-qubit IBM Sherbrooke superconducting quantum processing units (QPU) to explore the tradeoff between generalizability, sensitivity of circuit design to parameters, noise resilience, resource planning, and efficient qubit usage insights.

Keywords— GHZ, Qiskit, Quantum Circuits, Quantum Fourier Transform (QFT), Superconducting qubits, W state

# I. INTRODUCTION

Since the Bell experiment examined whether quantum mechanics permits local hidden variables [1], the standard quantum circuits, viz. Bell state, transpired later with quantum circuit form [2], and so on, for quantum computing practice. Quantum devices form the foundation for utilizing specialized hardware in quantum computing. For example, the states of a spin 1/2 particle can be used as qubit basis states by designating the +1/2 spin state as basis state  $|0\rangle$  and the -1/2 spin state as basis state  $|1\rangle$ . The photon polarization can also be used as a qubit by designating the horizontal polarization as the basis state  $|0\rangle$  and the vertical polarization as the basis state  $|1\rangle$ . Energy levels of atoms or quantum dots can be used as qubit states. The presence of an electron at energy level  $E_0$  is linked to the basic state  $|0\rangle$ . The existence of an electron at energy level  $E_1$  is associated with the fundamental state  $|1\rangle$ . Superconducting qubits in quantum computing research have set a new paradigm. Fixed-frequency

qubits, whose distinctive features are predetermined at manufacture, are used in IBM Quantum systems. In these systems, the cross-resonance (CR) gate is the two-qubit entangling gate, in which the control qubit is operated at the resonance frequency of the target qubit [3]. An all-microwave two-qubit gate uses a set frequency at ideal bias points. The gate may be adjusted by varying the amplitude of microwave radiation on one qubit at the transition frequency of the other, and it does not require any further sub-circuitry. Quantum process tomography shows an 81% gate fidelity, and we use the gate to create entangled states with a maximal extracted concurrence of 0.88 [4]. Superconducting rings are now being considered for use.

We are currently at a turning point in the development of quantum computing, where quantum systems have grown to the size and caliber required to address complex scientific issues beyond the scope of precise, brute-force classical approaches. We believe that current classical work should be combined with quantum elements and executed on heterogeneous quantum-classical platforms within a computational framework known as quantum-centric supercomputing (QCSC) to further this research. Quantum-computing elements in QCSC algorithms and architecture will provide a value that neither classical nor quantum computations alone can equal. Researchers will receive assistance in developing novel algorithmic breakthroughs with QCSC [5].

The transpiler rewrites them over several passes to optimize and convert circuits to the target instruction set architecture (ISA). This term, "transpiler," is used in Qiskit to emphasize the tool's role as a circuit-to-circuit rewriting tool, rather than a complete compilation down to controller binaries, which are necessary for circuit execution. However, another way to think of the transpiler is as an optimized compiler for quantum programs. Significantly reliant on the underlying quantum computer architecture, the ISA is the primary abstraction layer that separates the hardware from the program. A practical quantum computer that uses superconducting qubits, for instance, may have CNOT,  $\sqrt{X}$ , and RZ( $\theta$ ) rotations [6].

Additionally, circuits can be modified by Qiskit to work with various quantum platforms with varying instruction set designs, including superconducting or trapped-ion technologies, timings, error rates, and other limitations. Qiskit's Target class, an abstract machine model, may represent various quantum hardware types. The Target establishes a model for characterizing the accessible instructions on quantum hardware as well as the hardware's characteristics. Qiskit's retargetable transpiler can use this information to optimize the circuit for a specific piece of hardware [6].

IBM Sherbrooke and IBM Brisbane are equipped with 127 qubits of Eagle r3 architecture, featuring an echoed cross-reference (ECR) gate set, as well as Rx, Sx, and X gates, with Identity gates enabled on the QPU. A major quantum computing project in Canada includes the IBM Sherbrooke processor. It is run by PINQ<sup>2</sup> (Platform for Digital and Quantum Innovation of Quebec) and is located within the IBM Quantum System One installed at IBM Bromont, Quebec [7]. These are available from IBM Quantum platform [8] for creating and running quantum circuits.

# II. Quantum Circuits, Qubit Devices and Superconducting Qubits

Richard Feynman's postulation of a quantum computer [9] transpiring with the subsequent quantum algorithms viz. The Deutsch algorithm [10], Bernstein-Vazirani algorithm [11], Deutsch-Jozsa

algorithm [12], Shor algorithm [13], Grover algorithm [14], and Simon's algorithm [15] have enabled growing research interest over the years, with the advent of quantum hardware featuring qubit devices. Research interest in Superconducting Quantum Interference Devices (SQUID), and subsequent superconducting qubits including charge qubits, Josephson junction, molecular magnets, and discovery at the start of the 1990s that specific polynuclear molecular clusters based on d-block metals exhibit magnetic hysteresis at low temperatures, similar to that seen in bulk magnets working on the magnetism of molecules. Moreover, a second generation of molecular nanomagnets, based on mononuclear complexes with a single magnetic ion, typically a f-block metal, arose in the 2000s and also paves the way for undertaking novel directions in the interwoven regime of quantum devices and computing. Lanthanides have piqued the community's interest [16] that shows a promising direction while implementing the Grover algorithm. However, superconducting qubit devices gained momentum gradually. A Josephson junction between a nanometer-scale superconducting electrode and a reservoir creates a single-Cooper-pair box, an artificial two-level electronic system [17].

A qubit was created that is suitable for incorporation into a massive quantum computer and can be produced using traditional electron beam lithography. The two-qubit states have persistent currents in the opposite direction; the qubit is made out of a micrometer-sized loop with three or four Josephson junctions. Pulsed microwave modulation of the enclosed magnetic flux by currents in control lines yields quantum superpositions of these states. Entanglement of qubit information results from the regulated transfer of flux between qubits caused by the persistent currents via a superconducting flux transporter [18]. Over the past years, superconducting qubit performance has increased by several orders of magnitude. These circuits have not yet run into any strict physical limitations and benefit from the Josephson effect and the durability of superconductivity. However, creating error-corrected information processors with many of these qubits will require solving specific architectural issues, creating a new study area. For the first time, physicists will need to become proficient in quantum error correction to create and manage intricate active systems that are dissipative but always coherent [19].

IBM illustrates the adaptability of superconducting qubits in the extended quantum bus architecture for application towards a larger fault-tolerant quantum computing device using single-junction transmon qubits connected by two coplanar waveguide (CPW) resonators acting as the buses. Each qubit is coupled to its own distinct CCW resonator for independent readout and control [20].

Over the years, IBM Quantum has developed multiple generations of quantum computers, each advancing the capabilities of quantum computing. Modern superconducting quantum computers based on transmon qubits, selected for their scalability and controllability, are used to build these systems [21].

Some fundamental quantum circuits, such as the quantum Fourier transform (QFT), the Greenberger–Horne–Zeilinger (GHZ) state, and the W state, have evolved chronologically, leading to the current advancement of quantum computing research and applications, which are unsurprisingly used in IBM QPU.

# A. QFT circuit

Since the introduction of QFT in [13], Eq. 1 as given below, it is considered in many quantum computing applications, as in Eq. 1:

$$\frac{1}{\sqrt{q}} \sum_{c=0}^{q-1} e^{2\pi i a c/q} |c\rangle \quad (1)$$

The semiclassical (measurement-based) QFT concept uses classical feedforward (conditional phase corrections based on previous results) with one-by-one qubit measurements to circumvent controlled rotation gates. Implementing QFT effectively uses more classical post-processing and fewer quantum gates [22]. Further small-angle controlled-phase gate-omitting approximation QFT algorithms demonstrated that the QFT circuit can be truncated while remaining correct within an error bound  $\varepsilon$ , ignoring phase gates with minimal rotation angles. From  $O(n^2)$  to  $O(n \log n)$ , complexity decreases with exponential savings for high n [23]. In the quantum computing endeavour, later in a 2-qubit system with QCS, a MATLAB simulation tool, QFT, was simulated [24] in 2005. In Qiskit, QFT has been cited in different applications as [25], cited n-qubit shift operation in conjunction with others [26]. Mapping with different hardware on 5-qubit circuit QFT linear-depth solutions on several architectures, including IBM Heavy-hex, Google Sycamore, and 2D grid. A formalism for program synthesis to determine QFT mapping solutions using various standard structures [27].

Citing research that shows the benefit of dynamic quantum circuits for the quantum Fourier transform on IBM's superconducting quantum hardware, surpassing earlier reports across all quantum computing platforms with certified process fidelities of > 50% on up to 16 qubits and > 1% on up to 37 qubits [28].

QFT enhances efficiency in numerous ways, particularly in terms of resource flexibility. QFT-based arithmetic operations do not require extra qubits when working with arithmetic operations between quantum states and provided classical inputs. Instead, phase rotation gates are immediately supplied with classical information. A quantum-classical comparator based on the quantum Fourier transform (QFT) has been proposed. It has been expanded to compare modular arithmetic and two quantum integers. The suggested operators are ideal for qubit resources since they only need one ancilla qubit[29].

#### B. GHZ state circuit

When extended to quantum systems with at least three particles, it is demonstrated that the tenets of the Einstein-Podolsky-Rosen paper are incoherent. The proof shows that, even in the case of perfect correlations, the EPR program defies quantum mechanics [30] and subsequent papers [31], [32]. For an n-qubit system, the (2) is as written as:

$$\frac{1}{\sqrt{n}}(|0\rangle^{\otimes n} + |1\rangle^{\otimes n}) \quad (2)$$

A quantum control technique for the deterministic production and stability of the three-qubit GHZ state in the solid-state circuit QED system was described by extending the two-qubit Bell state to the three-qubit GHZ state [33].

Multi-qubit GHZ state generation and detection in circuit QED [34]. For the Greenberger-Horne-Zeilinger state distribution, a straightforward loss-tolerant procedure was cited [35].

It demonstrates several experiments supported by high-fidelity digital quantum circuits and presents a general approach for generating, maintaining, and modifying large-scale GHZ entanglement by use of a scalable methodology to generate genuinely entangled GHZ states with as many as 60 qubits for initialization [36].

A linear trend is observed in the decoherence rate of  $\alpha = (7.13 \text{N} + 5.54)10 - 3 \,\mu\text{s} - 1$  for up to N = 15 qubits, demonstrating the lack of super-decoherence, and a significant improvement in GHZ decoherence rates for a 7-qubit GHZ state following the implementation of dynamical decoupling. Furthermore, fully bipartite entangled native graph states on 22 superconducting quantum devices were created and described, all active qubits of the IBM Osprey 433-qubit device, with qubit counts as high as 414 qubits [37].

#### C. W state circuit

The set of truly trifold entangled states is divided into two sets that are unrelated under local operations assisted with classical communication (LOCC) when any nontrivial tripartite entangled state is transformed using stochastic local operations and classical communication (SLOCC) into one of two standard forms, either the GHZ state or another state as the W state [38]. For a n-qubit system, the generalized form is (3) as given by:

$$\frac{1}{\sqrt{n}} \sum_{i=1}^{n} |e_i\rangle \tag{3}$$

Where the i-th qubit is in state  $|1\rangle$  and every other qubit is in state  $|0\rangle$ , the symbol  $|e_i\rangle$  indicates a computational basis state. Fault-tolerant quantum computers repeatedly apply a four-step process: Execute a few one- and two-qubit quantum gates first. A selection of the qubits should then be subjected to a syndrome measurement. Third, determine whether and where errors occurred by performing quick classical computations. Fourth, use a corrective step to fix the mistakes. The exact process is used with fresh one- and two-qubit gates in the subsequent iteration [39].

To create infinitely huge qubit and qudit W states of any prime power size for any prime qudit dimension, the controlled H gate was constructed in any odd qudit dimension [40].

High-order W-state production using an integrated quantum circuit and extremely accurate characterization [41].

Multipartite entanglement is present in many inequivalent types of massive quantum systems. To carry out a variety of quantum protocols, states of arbitrary sizes in various classes must be prepared. Specifically, a class of quantum networking protocols is composed of W states [42].

# D. Many qubit circuits

A three-qubit nuclear magnetic resonance (NMR) quantum computer has been equipped with a quantum Fourier transform (QFT) to determine the periodicity of an input state. The realization of Shor's factoring and other quantum algorithms begins with the implementation of a QFT [43].

Quantum Circuit Initialization for 127 qubits initializes a quantum circuit (qc). Entanglement and the Use of QFT by the qubits are separated into clusters, each with ten qubits. A Quantum Fourier Transform converts a quantum state into its frequency domain for every cluster [44].

Examining the physical implementation of Shor's factorization technique on a Josephson charge qubit register reveals the methodology for the number 21, which serves as a general approach to factor a composite integer of any size. When a limited number of qubits is available, considering both the algorithmic and physical constraints for an optimal implementation, these essential characteristics are comprehensively analyzed, connecting Shor's algorithm to its physical implementation with Josephson junction qubits. Typically, these facets of quantum processing are the focus of distinct research communities. This speeds up the method by breaking down the quantum circuit into customized two-and three-qubit gates, and we use numerical optimization to determine their physical realizations to satisfy the strict criteria imposed by a short decoherence period [45].

The layout in a quantum circuit, provided by Qiskit, includes any related circuit layout details. An optional TranspileLayout object is included in this attribute. Usually, this is set on the output of PassManager or transpile().run() to save data regarding the permutations that transpilation causes on the input circuit. A final layout, which is an output permutation brought on by SwapGates added during routing, and an initial layout, which permutes the qubits according to the chosen physical qubits on the Target, are the two kinds of permutations brought about by the transpile() function [46].

The QAOA problem, with each node being used as a qubit in a multi-qubit quantum computer, has been used for the max-cut problem solution [47].

Eight quantum bits apiece make up the 4x4 unit cells that house the array of superconducting quantum bits. Each of the four qubits in a unit cell's left-hand partition (LHP) is connected to every other qubit in the right-hand partition (RHP), and vice versa. The corresponding qubit in the LHP (RHP) of the unit cells above and below (to the left and right of) a qubit in the LHP (RHP) is also connected to it. The edges between qubits, which are labelled 0–127, stand in for couplers with configurable coupling strengths. Whereas vacancies denote qubits under calibration that were not utilised, grey qubits represent the 115 available qubits [48].

A complete quantum solver is presented that regularly provides accurate answers for issues involving up to 127 qubits and surpasses any existing alternative for binary combinatorial optimisation problems on gate-model quantum computers. We show that Max-Cut cases for random regular graphs with

different densities can be correctly solved with up to 120 qubits when the graph topologies are not matched to device connectivity [49].

Superconducting qubits have advanced significantly in recent years. The number of qubits has risen with system sizes, gradually increasing from 127 to 433 qubits, and thousands are in the pipeline. The EFTQC-to-FTQC transition is distinguished by its capacity to handle considerable problem instances (e.g., encoding 10,000 logical qubits using only 109 physical qubits), whereas the NISQ-to-EFTQC transition is characterized by its sufficient qubits to implement fault-tolerant non-Clifford operations (e.g., T factories) [50].

Cross-resonance pulses are scaled to do a framework for the pulse-efficient transfer of circuits in noisy quantum hardware, and each pulse is exposed as a gate to eliminate unnecessary single-qubit transpiler operations. Importantly, it produces better outcomes than a CNOT-based translation without the need for extra calibration. Because of this pulse-efficient circuit translation, the user can make greater use of the short coherence time without having to be aware of the specifics of each pulse [51].

#### E. Error correction

One intriguing finding in real-world quantum hardware-based computation is that circuit complexity may affect dependability. The number of gates that apply to a bit sequence depends on the number of ones (1) in it. [52].

A method for compensating for the noise produced during a quantum computation is called quantum error mitigation. It is the key to making quantum computing usable and a necessary component of scalable quantum computing. One popular method is to use software to correct for inaccuracies in the raw results while modelling the device noise during execution. The quantum utility article recently introduced techniques like Probabilistic Noise Cancellation (PNE) and Zero Noise Extrapolation (ZNE). Error Through postprocessing, mitigation lowers the final result's error. Quantum error correction ensures that the data remains at the desired value or is automatically adjusted to the value that should be there at that precise instant. It will be necessary for the qubits to exhibit fault tolerance using quantum error-correcting processes to gain a computational advantage in larger-scale systems. Error correction/mitigation software and hardware solutions are being developed. [53].

The now-defunct Ignis introduced the repetition code and its Qiskit implementation. It is a component of Qiskit-Ignis' topological\_codes module, which makes it relatively easy to add new codes and decoders because of its modular nature. [54].

Recognizing and resolving issues when working with quantum systems is crucial for fault-tolerant quantum computing. Unlike classical bits, which are solely impacted by digital bit-flip mistakes, quantum bits are susceptible to many flaws. This is an essential part of any complete quantum error-correcting code. The data must be encoded into a quantum error-correcting code to achieve a fault-tolerant quantum computer, which is a challenging problem. Because direct information extraction typically destroys the system, ancillary syndrome systems must employ non-demolition measures to preserve the encoded state, which complicates matters. [55].

There are numerous technologies for quantum computing. Despite several attempts to compare them, applied research is necessary due to the variations in their implementation. The essay provided updated considerations to help users choose between technologies and identify profitable research areas. Over time, advancements in technology's accuracy and speed have been demonstrated using a chemistry example. Confidence in the preparation of the anticipated arrival of a substantial Quantum Advantage is increased by recent and upcoming developments. In sectors where it is a business priority, networks and industrial consortia collaborate to identify key issues. Resources to help with the transition to quantum computing are described. Recognizing that it will take time for domain experts to develop the necessary skills to find and utilize appropriate technology is crucial; depending on the application, this can take two to three years. [53].

In light of the above, it is apparent that the three fundamental quantum circuits often used for different applications, either standalone or integrated with other parameters, have the potential to create relatively bigger circuits in terms of qubit use. In the noisy environment of NISQ, error correction is also a technique adopted to gain confidence in the output of real hardware.

This work contributes to the modelling of individual QFT, GHZ, and W state quantum circuits, ranging from four to ten qubits, using Qiskit simulators and IBM Sherbrooke's 127-qubit superconducting quantum processing units. This reveals the differences in circuit layout, including depth, width, and number of qubits, for hardware compatibility. Each four to ten qubits circuit was run with 4096 shots in the simulator and QPU Sampler for comparison. The novelty of this paper lies in comparing the outcome in the NISQ era with metrics to observe the difference between the runs of twenty-one baseline quantum circuits and their counterpart transpiled circuits from the simulator and superconducting QPU for different qubit systems and identifying the scope of applying error correction thereof.

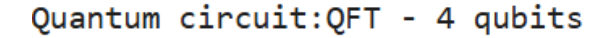
#### III. Circuits in the Simulator and QPU

In the qiskit SDK IBM quantum ecosystem, using (1), (2) and (3), three n-qubit circuits of QFT, GHZ, and W state have been built for values of n from 4 to 10, and initial state graphs obtained. Each circuit is run through the Statevector Simulator for 1024 shots to yield the state graphs. The Bloch sphere is used to compare the before-and-after measurements. Aer Simulator, through subsequent runs of each circuit for 4096 shots, was made hardware compatible by an available technique called transpilation. The transpiled circuits were then compared with available Sampler runs, specifically with IBM Sherbrooke, which proved to be the least busy available QPU with 127 qubits. The results of Aer Simulator and Sherbrooke QPU are then compared with metrics of Total Vector Distance (TVD), KL Divergence, Jensen-Shannon Divergence, and Hellinger distance for evaluating pattern proximity or divergence to identify if all the qubit-based circuits have any meaningful information ready for extraction for any particular qubit-based system. Based on the best qubit number, each quantum circuit for either category is presented in a bar chart, providing insight for gaining an understanding. It takes stock of the findings and the Sampler based on resilience, further compared with the Estimator technique. An error mitigation facility called dynamic decoupling is further applied to the best qubit based on each type of quantum circuit and compared. The results of total 21 circuits run through simulators and IBM superconducting physical qubits Sherbrooke QPU succeeded by a selected few circuits for error mitigation, were further discussed, comparing with the difference between the

standard circuits and transpiled circuits for finding any trade-off in circuit design and hardware performance and concluded for possible future direction and discussing any limitation of the study.

# IV. Outcome Visualization

Using Qiskit, 4-qubit quantum circuits for QFT, Fig. 1, 2, and 3, GHZ state, and W state, depict the use of respective applicable gates and measurements. The corresponding circuits were transpiled with the IBM\_Sherbrooke backend, as described in Figs. 4, 5, and 6, respectively, showing the difference in resulting layouts for mapping onto real quantum hardware. The circuit depth and width are adjusted through transpilation, ensuring they match the physical qubits.



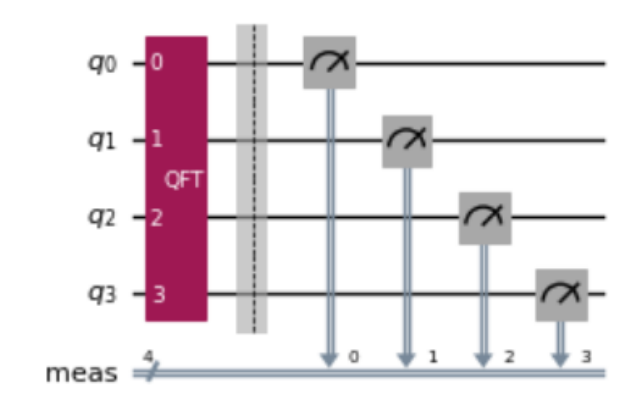


Fig. 1. Quantum circuits with 4 qubit: QFT

Quantum Circuit: GHZ state - 4 qubits

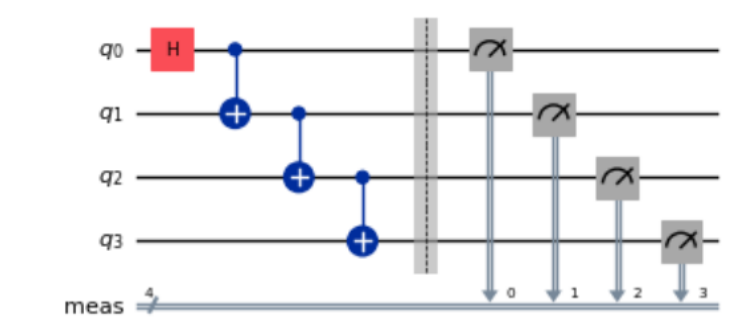


Fig. 2. Quantum circuits with 4 qubit: GHZ

# Quantum circuit: W state - 4 qubits

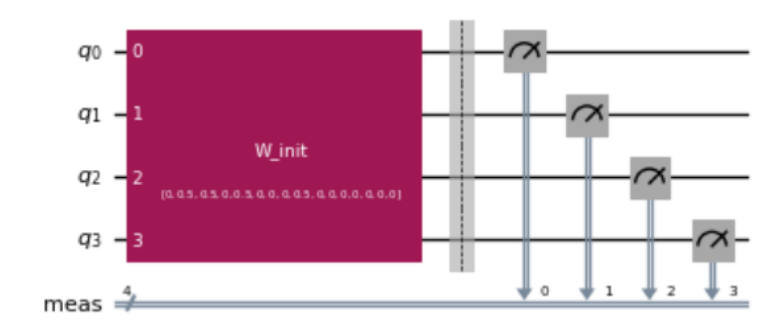


Fig. 3. Quantum circuits with 4 qubit: W state

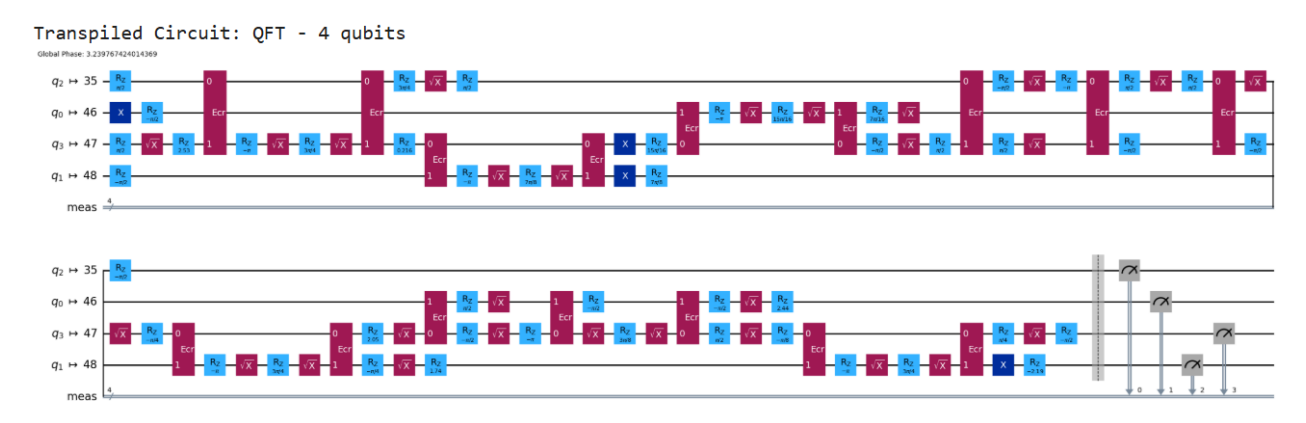


Fig. 4. Transpiled Quantum circuits with 4 qubit: QFT.

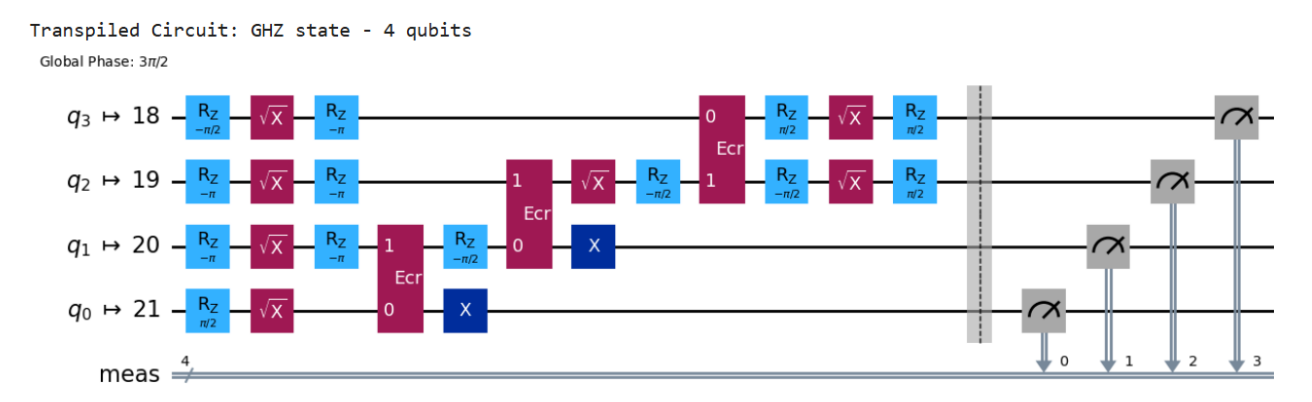


Fig. 5. Transpiled Quantum circuits with 4 qubit: GHZ

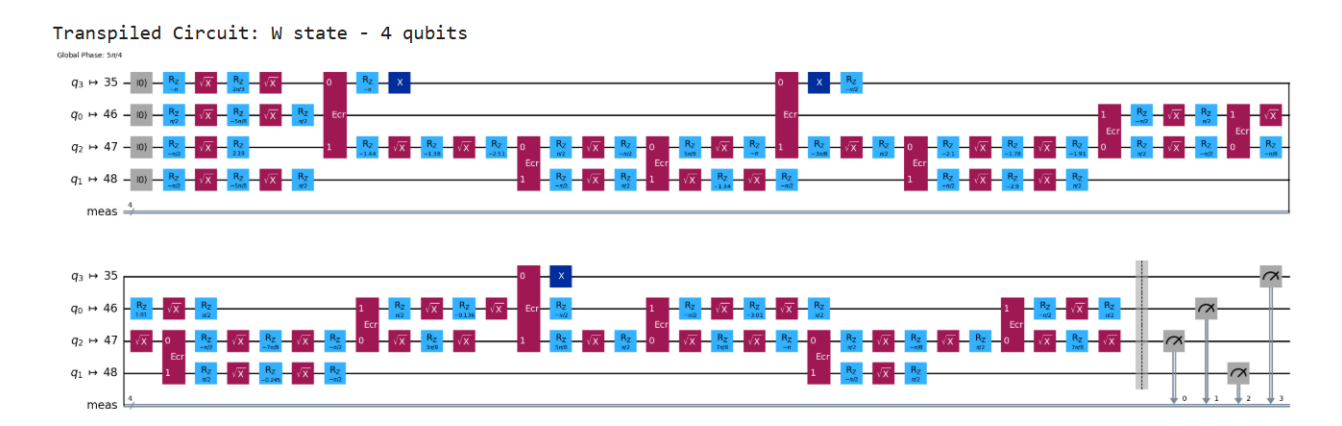


Fig. 6. Transpiled Quantum circuits with 4 qubit: W state.

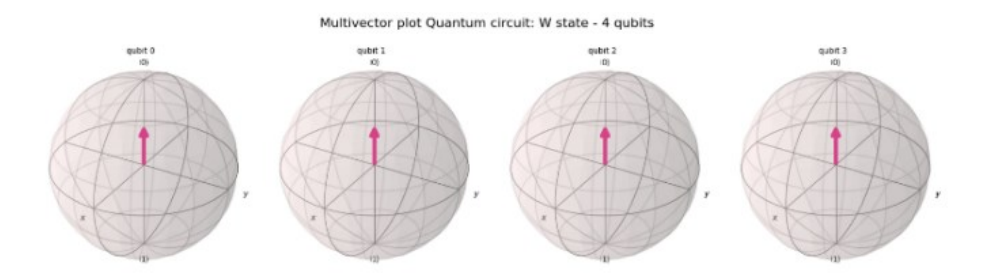


Fig. 7. 4-qubit W state multi-vector plot from statevector before measurement

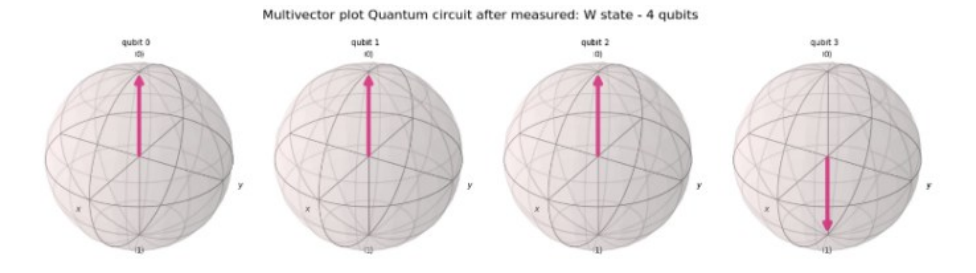


Fig. 8. 4-qubit W state multi-vector plot from state vector after measurement.

Fig. 7 and 8 depict the 4-qubit W state before and after measurement through the Aer Statevector simulator, after 1024 shots were run, respectively. The red arrow, initial state, Fig. 7, indicates the state vectors pointing towards the Z direction with no superposition or entanglement; however, shorter lengths resemble a mixed state in the  $|0\rangle$  state, Fig. 8. In comparison, the post-measured classical state of qubit 3 is evident from the red arrow pointing towards state  $|1\rangle$ , indicating a difference in coherence from the pre-measure state.

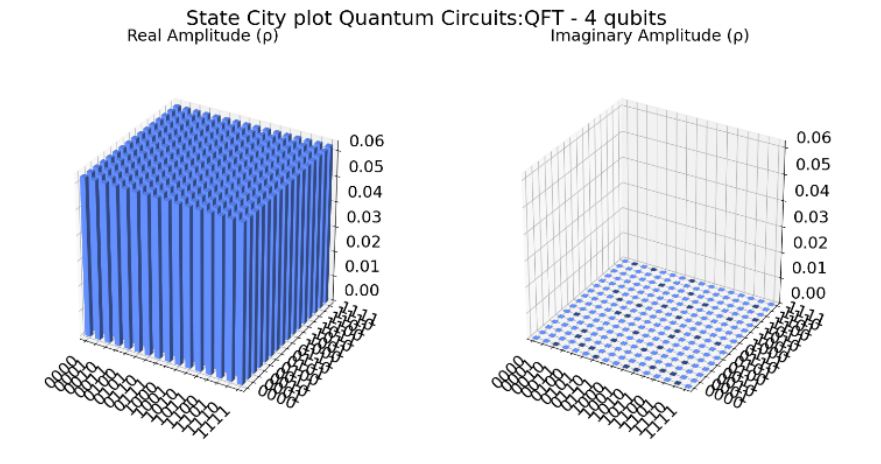
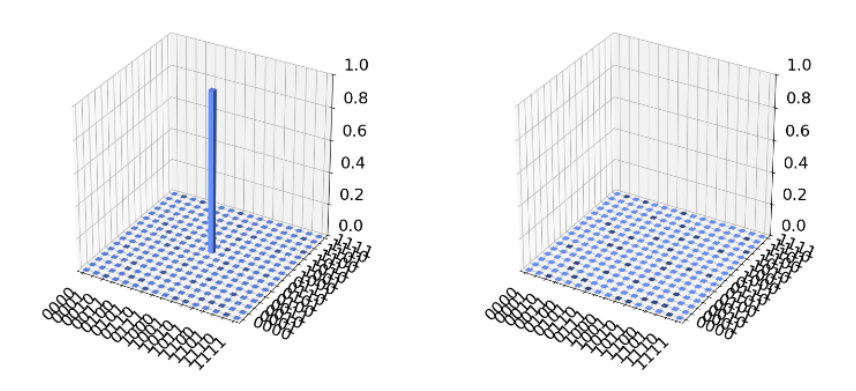
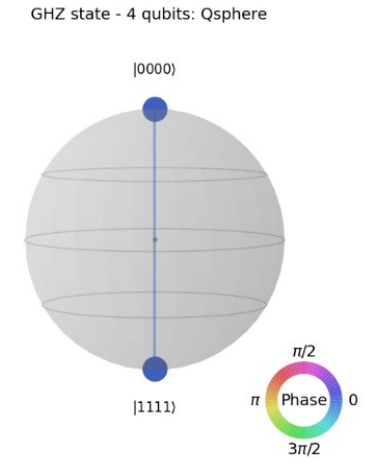


Fig. 9. 4-qubit QFT state city plot from state vector before measurement. State City plot Quantum Circuits after measured: QFT - 4 qubits Real Amplitude ( $\rho$ )



**Fig. 10.** This 4-qubit QFT state city plot from statevector after measurement.

Fig. 9 reveals a 4-qubit QFT system where the before measurement of each state has a probability of 0.06 in the 4-qubit system, which collapses to the classical state of |0001⟩, Fig. 10, post measurement.



**Fig. 11.** GHZ state – 4 qubit Qsphere from statevector before measurement.

Fig. 11 and 12 depict a 4-qubit GHZ state, a classic pure superposition, and a highly entangled state that collapses to |1111\(\rightarrow\), respectively.

GHZ state - 4 qubits: Qsphere after measured

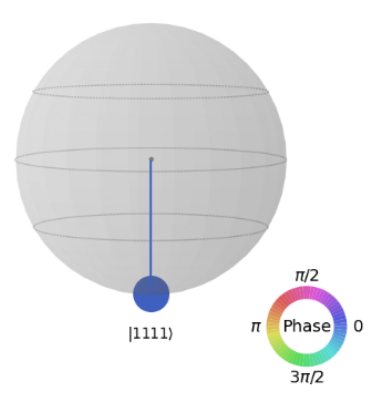


Fig. 12. GHZ state – 4 qubit Qsphere from statevector after measurement

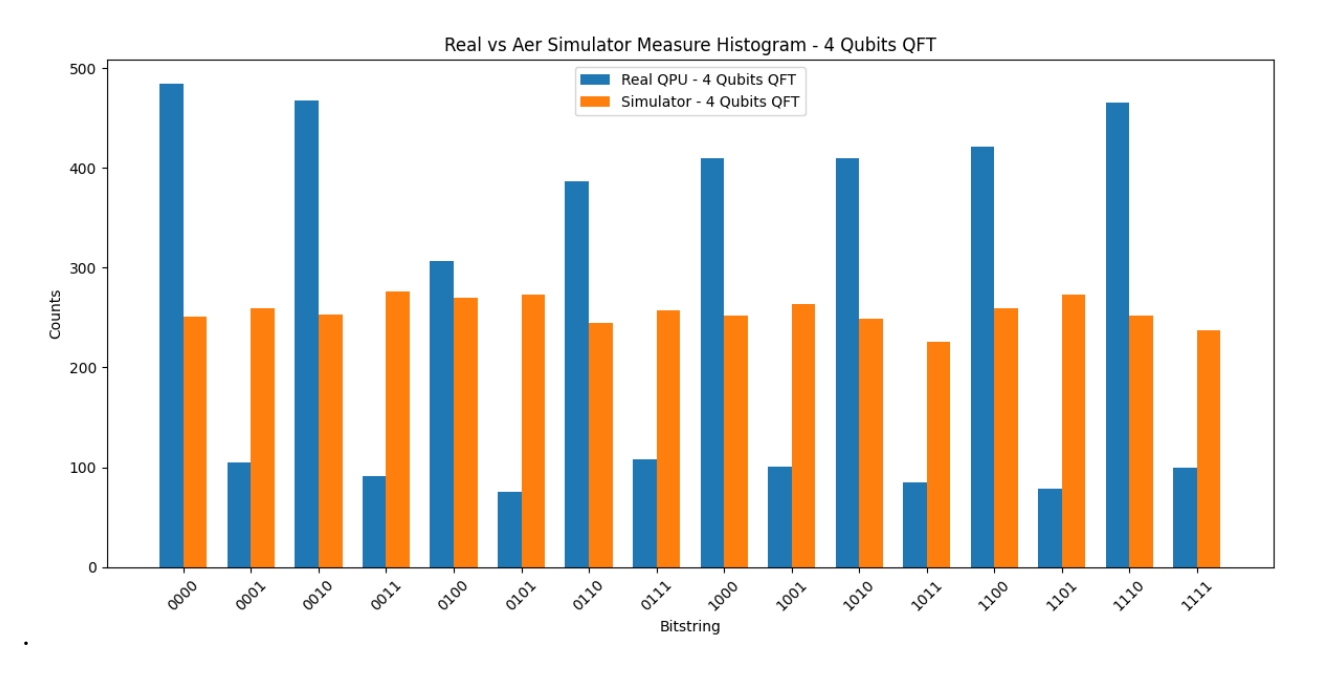


Fig. 13. 4 Qubit QFT Aer Simulator and IBM Sherbrooke histogram.

Figure 13 compares Aer Simulator and IBM Sherbrooke count results of 4096 shots for each 4-qubit QFT circuit post measurement state. The simulator results are mostly uniform, while the taller and shorter bars for some states in QPU count indicate the difference in results in contrast.

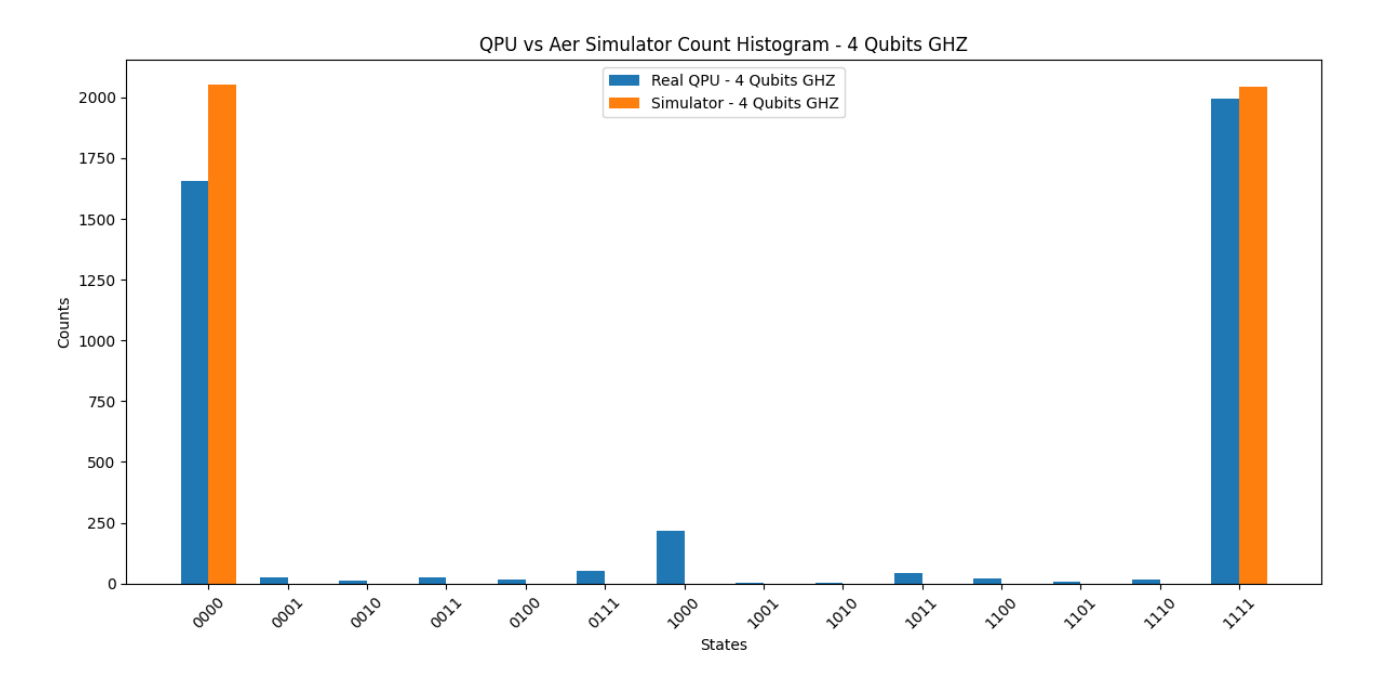


Fig. 14. 4 Qubit GHZ Aer Simulator and IBM Sherbrooke histogram

Fig. 14 reveals the stark difference in simulator and QPU counts with the introduction of noise in shorter blue bars, while the simulator results are consistent for 4-qubit GHZ states.

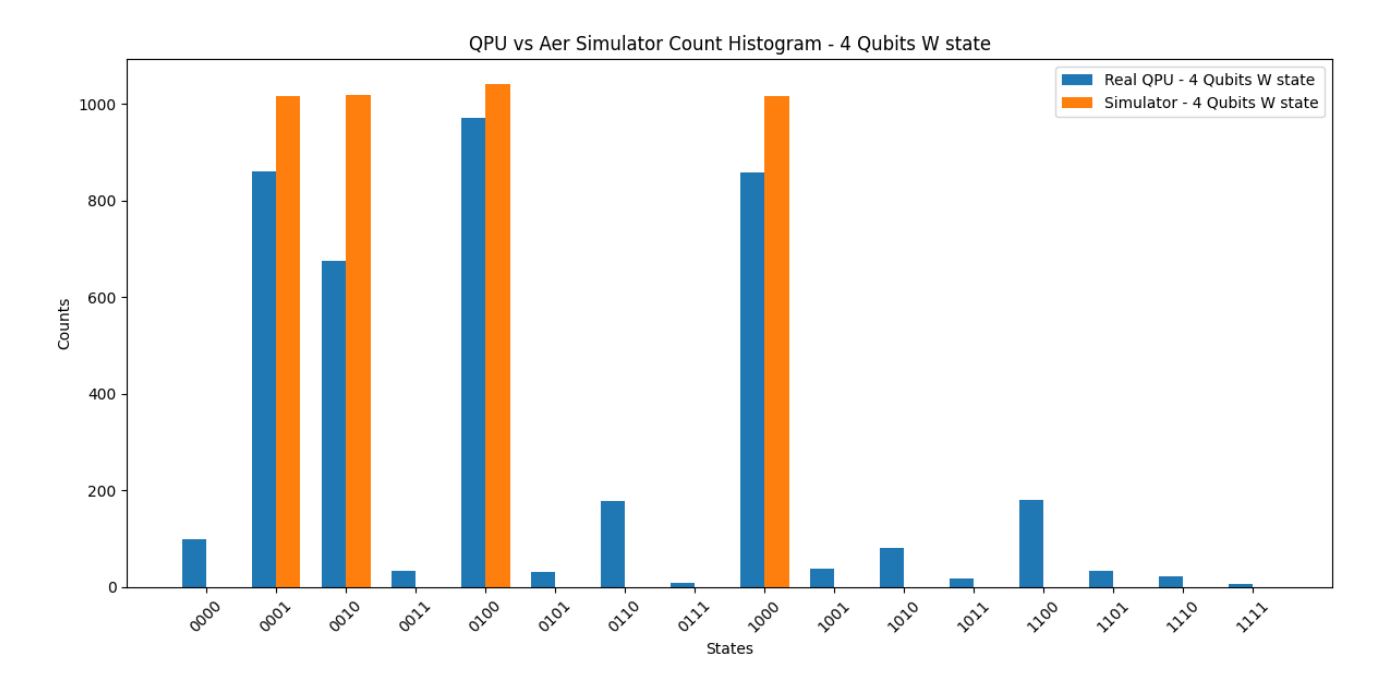


Fig. 15. 4 Qubit W state Aer Simulator and IBM Sherbrooke histogram

Fig. 13 depicts a 4-qubit W state in symmetric superposition, with each  $|1\rangle$  state having nearly equal counts as 1 qubit while others are in  $|0\rangle$ , as per Aer Simulator results. This differs from the QPU results due to noise in other states, as indicated by the short blue bars. Therefore, as is clear from the above Fig., QPU runs for 4-qubit systems yield noise in the QPU outcome compared with the simulator results. In this follow-up, the circuits are run through subsequent qubit systems, viz., 5 to 10, and the comparative results further indicate significance.

TABLE I

Qubits to Classical and Quantum Fourier Transform Comparison

Qubits	Classical FFT Vectors	Quantum QFT Qubits
--------	-----------------------------	-----------------------

3	8 complex numbers	3
10	1024 complex numbers	10
20	1 million+ entries	20 qubits
30	1+ billion amplitudes	30 qubits

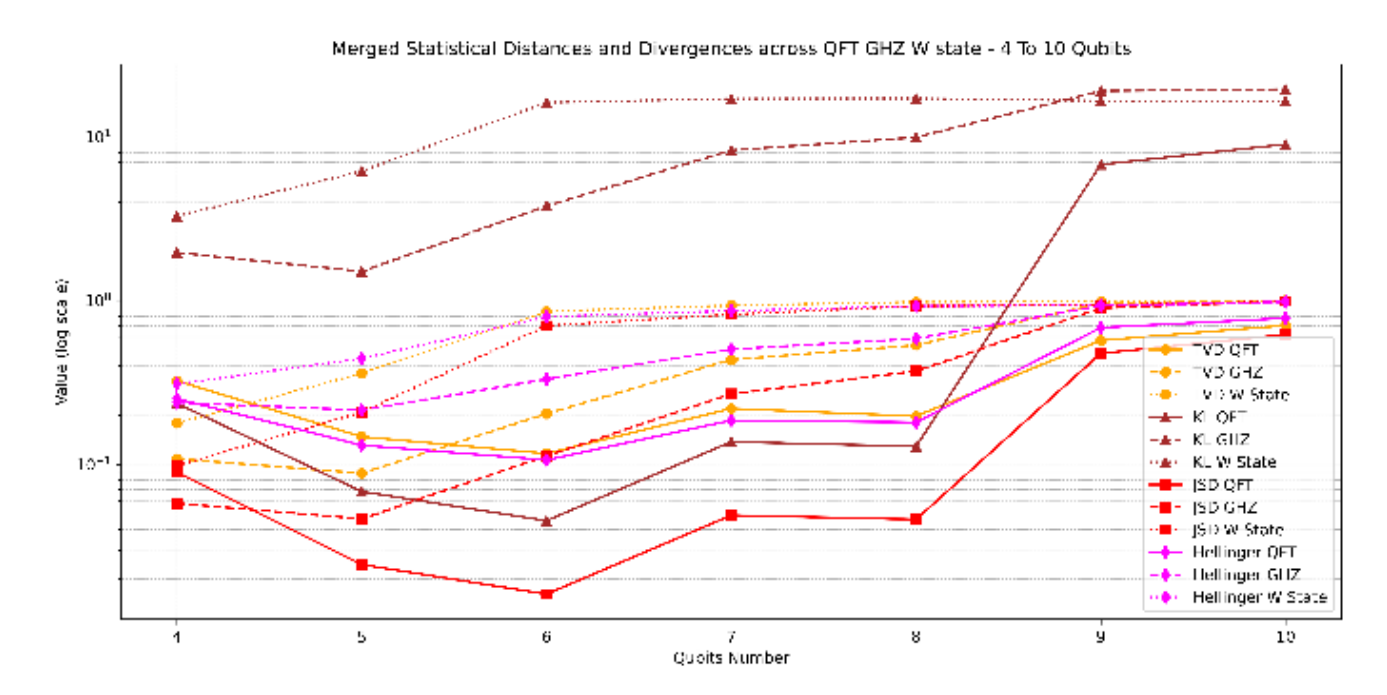
Table I provides 2<sup>n</sup> basis states, where n is the number of qubits, equivalent to corresponding amplitudes that can be represented simultaneously in the quantum Fourier transform due to superposition. This holds for 30 qubits, up to a billion, a stark contrast with classical computation limitations, highlighting the exponential growth. Table II further illustrates that the RAM size requirement for qubits increases, with 30 qubits requiring 16 GB and 37 qubits necessitating an astonishing 2048 GB, underscoring the need for quantum processors.

TABLE II
Required RAM size against qubits

	RAM Limit (GB)	Qubits
0	16	30
1	32	31
2	64	32
3	128	33
4	256	34
5	512	35
6	1024	36
7	2048	37

Table II further illustrates that the RAM size requirement for qubits increases, which for 30 qubits requires 16 GB, and for 37 qubits, astonishingly, 2048 GB, necessitating a simulator size that matches, rather than justifies, the use of quantum processors.

The quantum circuit outcomes from 4 to 10 qubits have been plotted on a logarithmic scale for comparison. Fig. 16 reveals that the metrics exhibit saturation or stabilization beyond six qubits, except for the KL distance. Individually, for QFT - six qubits, GHZ – 5 qubits, and W state – 4 qubits exhibit all four metrics at their lowest compared to others. This implies that the simulation and QPU run closely resemble the outcome, being the threshold for the individual quantum circuits, which requires almost no error correction. However, for QFT and GHZ above 9 qubits, the graphs tend to converge except for the W state, where the stabilization reaches from 6 qubits. The scope of error correction using available techniques in the IBM cloud, namely dynamic decoupling, gate twirling, and M3 techniques, appears to be the most effective for improving the circuit's outcome.



**Fig. 16.** QFT, GHZ & W state -4 to 10 qubits - Different metrices plot on qubit number and values in log scale

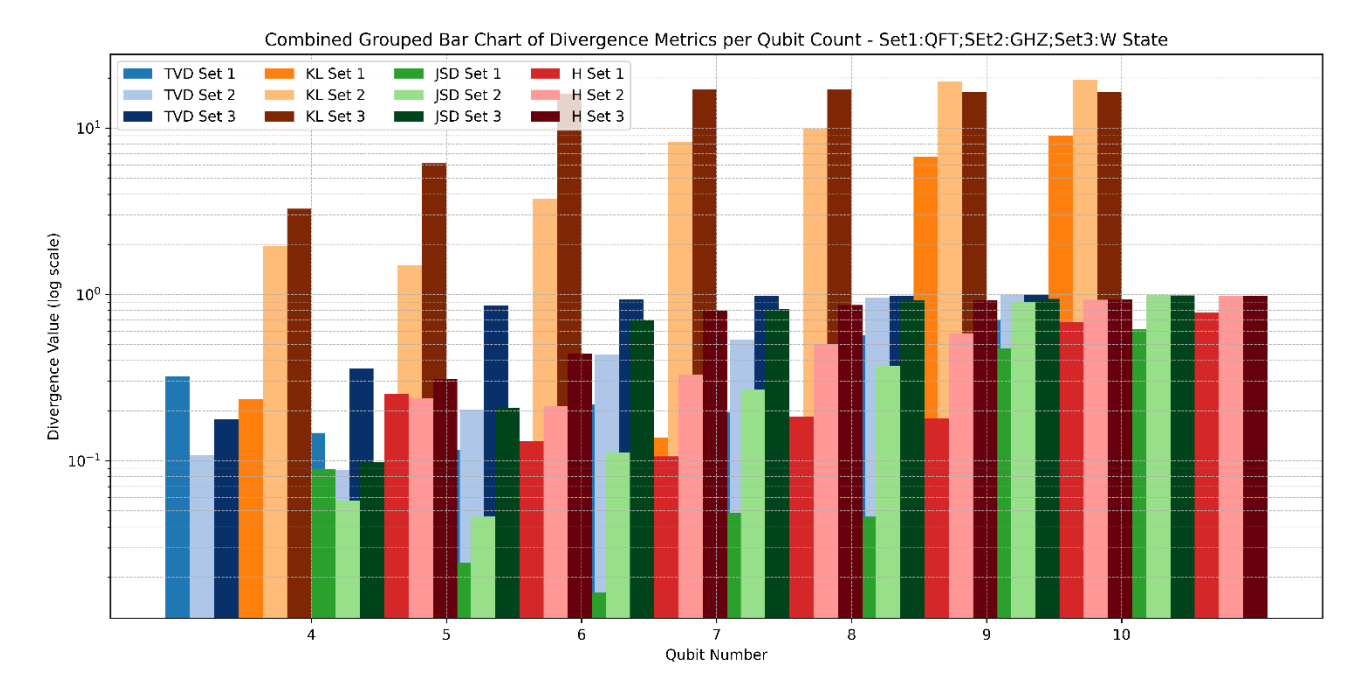


Fig. 17. Different Metrics comparison plot.

Based on Fig. 16, the metric values calculated for QFT-6 qubits, GHZ-5 qubits, and W state 4 qubits and produced in the subsequent figures 17. The Hellinger distance for QFT-6 qubits appears the minimum of 0.016, implying proximity of results in the aer simulator and QPU. These levels considered identical for comparison in the sense of Sampler without error correction compared with Estimator, a better candidate for adopting in a QPU run.

TABLE III

QFT quantum and transpiled circuit details

circ uit	de ph	wid h	mea sure men ts	gat es	barri ers	no. of qubit s		
Quan	Quantum circuit							
4	2	8	4	1	1	4		
5	2	10	5	1	1	5		
6	2	12	6	1	1	6		
7	2	14	7	1	1	7		
8	2	16	8	1	1	8		
9	2	18	9	1	1	9		

10	2	20	10	1	1	10		
Trans	Transpiled quantum circuit							
4	75	131	4	103	1	127		
5	102	132	5	168	1	127		
6	150	133	6	283	1	127		
7	234	134	7	406	1	127		
8	251	135	8	529	1	127		
9	285	136	9	675	1	127		
10	401	137	10	980	1	127		

TABLE IV

GHZ quantum and transpiled circuit details

circ uit	de ph	wid h	mea sure men ts	gat es	barri ers	no.of qubit s	
Quant	um ci	rcuit					
4	5	8	4	4	1	4	
5	6	10	5	5	1	5	
6	7	12	6	6	1	6	
7	8	14	7	7	1	7	
8	9	16	8	8	1	8	
9	10	18	9	9	1	9	
10	11	20	10	10	1	10	
Transpiled quantum circuit							
4	12	131	4	23	1	127	
5	14	132	5	29	1	127	

6	20	133	6	44	1	127
7	21	134	7	48	1	127
8	22	135	8	51	1	127
9	25	136	9	60	1	127
10	31	137	10	73	1	127

TABLE V
W state quantum and transpiled circuit details

circ uit	de ph	wid h	initi alize	me asu re me nts		no. of gates
Quan	tum c	ircuit				
4	2	8	1	4		4
5	2	10	1	5		5
6	2	12	1	6		6
7	2	14	1	7		7
8	2	16	1	8		8
9	2	18	1	9		9
10	2	20	1	10		10
Trans	spiled	quant	um circ	cuit	•	
4	4	65	31	4		99
5	5	155	132	5		278
6	6	349	133	6		323
7	7	737	134	7		749
8	8	182 6	135	8		3446

9	9	345 5	136	9	7162
10	10	708 3	137	10	1362 6

Tables III, IV, and V tabulate the complexity of the quantum base circuit and the transpiled circuit through the QPU backend. IBM Quantum offers an open-source basis, including some QPUs, such as the 127-qubit Brisbane, Sherbrooke, and Kyiv, for limited use of 10 quantum minutes per registered user ID. The base circuit's number of qubits is automatically compatible with 127 qubits. The width often exceeds 127 qubits, implying the use of logical ancilla qubits for computational purposes besides the physical 127 qubits. The number of depths and gates changes is remarkable depending on the circuit complexity, as shown in Table V. For 10-qubit systems, the numbers go as high as 7083 and 13626, the maximum. The intricate circuit design complexity is apparent in addressing a complex real-world problem.

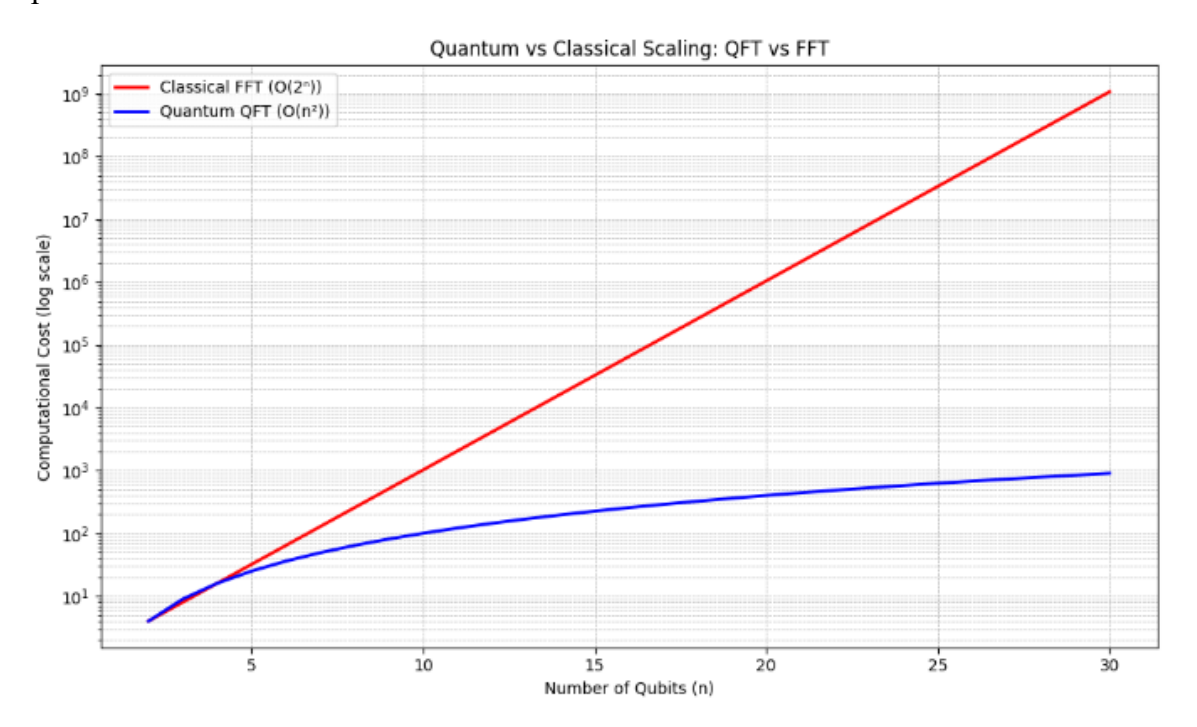


Fig. 18. QFT & FFT: Quantum and classical computational cost.

Compared with other quantum basic circuits used in this work, the use of QFT appears overall encouraging for building quantum circuits to address real-world domain-specific problems, nonetheless, depending on the problem statement and domain, a higher-qubit real hardware QPU should be used instead.

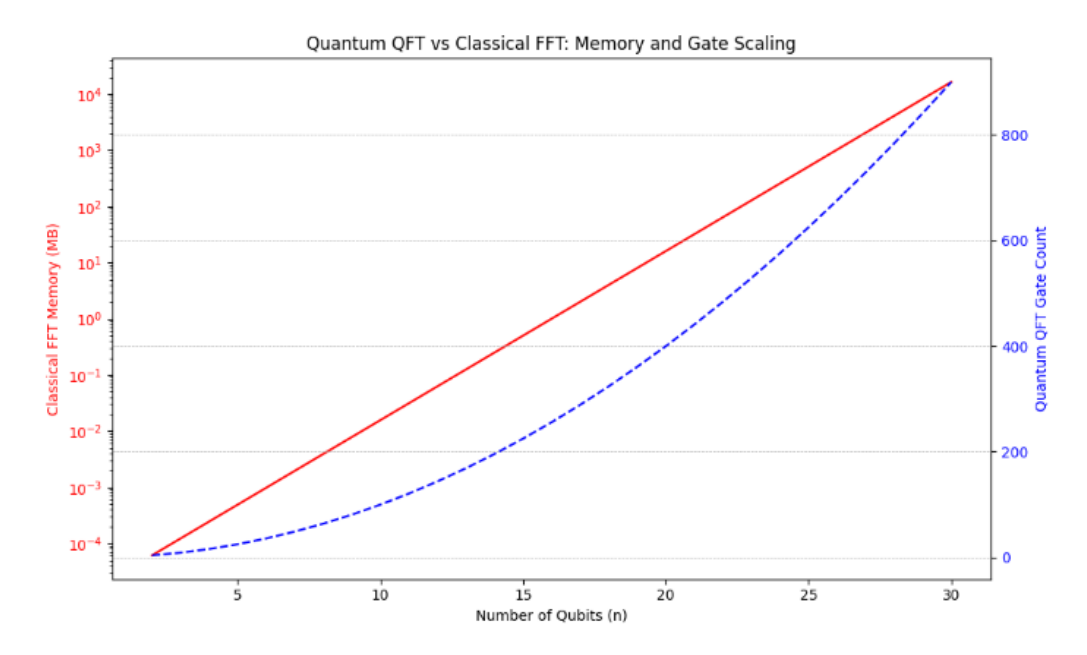


Fig. 19. QFT & FFT: Quantum and classical memory.

Fig. 18 and 19 reveal the quantum advantage in scaling and gate counts compared to classical QFT with increased qubits. Using a simulator provides a scope for baseline calculation; however, with the increase in the number of qubits, the memory increase will necessitate an increase in computational hardware resources. Hence, a real quantum computer could offer an advantage if error mitigation is addressed. In a real-world scenario, using a quantum circuit for addressing problems requires realistic data encoding, which has its complexity and type depending upon the scenario of computing or machine learning for finding a trade-off between computational resources and time of computation [56], [57].

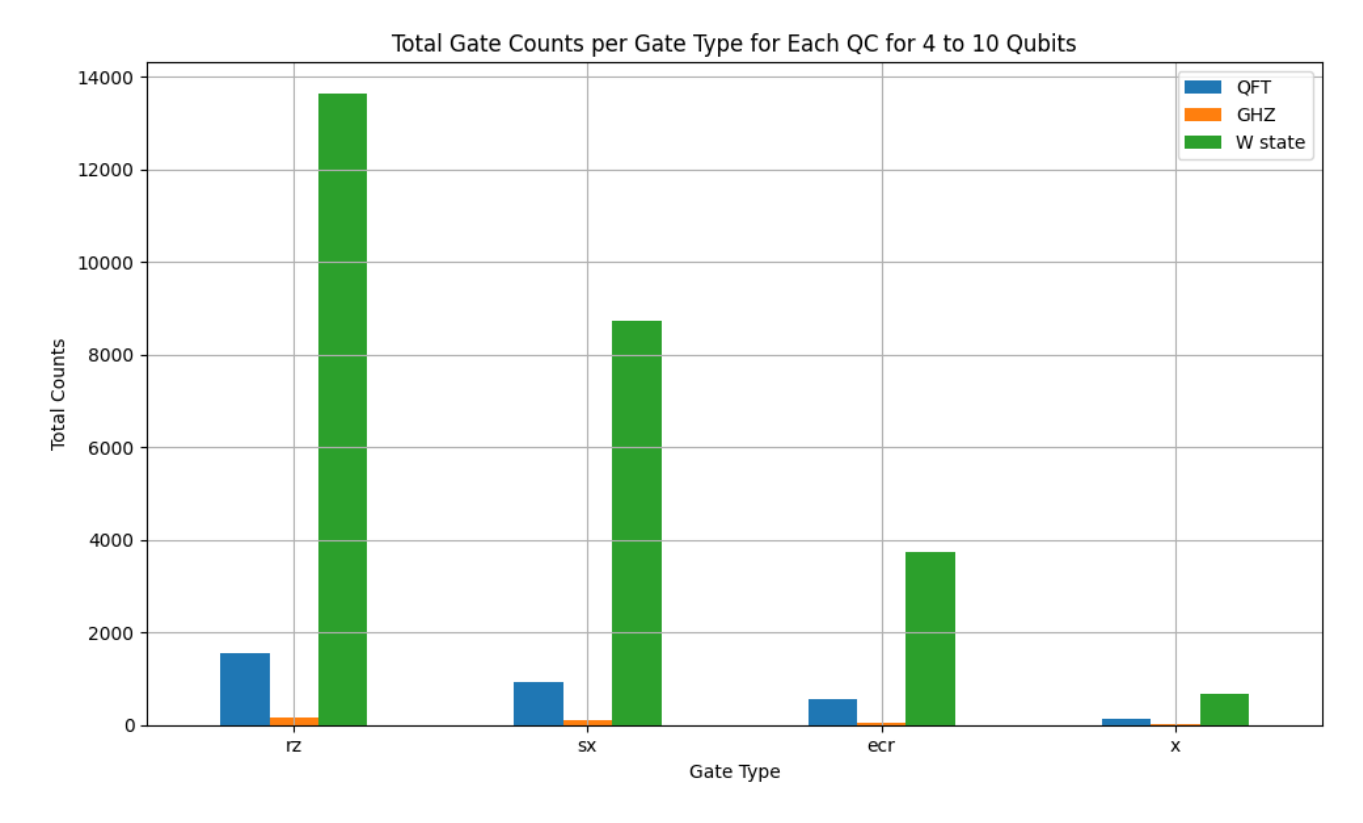


Fig. 20. Transpiled circuits and Gate Type comparison

Fig. 20 reveals the transpiled circuits gate comparison in superconducting physical qubits, breaking down the numbers from Tables III to V. All gate operations are dominated by W state, particularly rz, which rises to 13,623, far higher than OFT and GHZ qubit systems. The fact that GHZ constantly displays the lowest gate values may suggest that it is utilized for circuits with less complexity or depth. Since gate x is a simple gate frequently substituted by decompositions in practical circuits, it is expectedly to be the least used of all the circuits. This gate distribution may reflect each quantum circuit's hardware calibration properties, target application, or circuit complexity through a superconducting-based QPU. The work demonstrates how the quantum circuit layouts, when intended to run on superconducting quantum hardware, are changed through transpilation, introducing additional gates and their types to make them compatible with the physical qubits. The comparison of the width and number of qubits also indicates additional logical qubits configured as necessary. As a result, the number of qubits, gates, and operations changes profoundly compared to the circuits used for simulation. Moreover, depending on the type of base circuit's complexity, the degree of noise in the results is contingent upon the increase in the number of qubits. In contrast, the maximum number of available physical qubits remains fixed. For various qubit systems, the difference in results of the simulator and QPU identifies the need for error correction as a direct consequence of the number of qubits in base circuits. The work is limited to 127 qubit processors, which is the limitation of this work. This work opens up possibilities for future research using higher-end quantum processors that have a larger number of physical qubits.

#### V. Conclusion

Owing to their uniqueness, all three circuits, either in standalone or in conjunction with other qubit subsystems, i.e., QFT, GHZ, and W state, have found typical applications in various domains, from quantum communication, optimization, and many others. However, the number of qubits varies depending on the type of application in the respective domains, while addressing a domain-specific problem, depending on the size and complexity. In superconducting qubit-based quantum processing units, this work helps gain insight for making broader circuits based on basic circuits to create a system of possible sub-systems for extracting the quantum advantage in computing by building circuits with a larger number of qubits. As for a greater number of qubits, the simulator's use will be limited by the increasing RAM size; the study's outcome should be advantageous while planning in tandem with layout details for compatibility with the hardware architecture of physical superconducting qubits in the IBM quantum system endeavor. While quantum circuits with a greater number of qubits when required should be realistically addressed, for further application based on the use case and data size, obviously, viz. QML, where several variables are involved, will provide inevitable. Building quantum circuits from scratch using the standard and proven basic circuits of different qubit systems, either standalone or in integration with other gates and subsystems, for further domain-specific applications, entails meticulous planning of layouts and optimization. Moreover, in the NISQ era, each circuit must comply with IBM quantum processing units to run efficiently in the cloud. As such, transpilation has been made mandatory before job application and thus requires a thorough understanding of the impact of use in a particular problem. The optimization of circuit depth, width, and gate operations is crucial for a specific application. So, finding a trade-off for planning purposes is a requirement. Nonetheless, the study provides a scope for gaining fundamental insight for preparing quantum circuits, keeping the given finding trade-off between hardware performance, computation complexity, resource allocation planning, robustness of noise, and planning for error mitigation post raw run for envisaging the quantum advantage in computing.

# References

- [1] J. S. BELL, "on the Einstein Podolsky Rosen Paradox," *John S Bell Found. Quantum Mech.*, vol. 1, no. 3, pp. 7–12, 2001, doi: 10.1142/9789812386540 0002.
- [2] C. H. Bennett, G. Brassard, C. Crepeau, R. Jozsa, A. Peres, and W. K. Wootters, "Teleporting an Unknown Quantum State via Dual Classical and Einstein-Podolsky-Rosen Channels," vol. 70, no. 13, 1993.
- [3] P. Nation, H. Paik, A. Cross, and Z. Nazario, "The IBM Quantum heavy hex lattice." [Online]. Available: https://www.ibm.com/quantum/blog/heavy-hex-lattice
- [4] J. M. Chow *et al.*, "Simple All-Microwave Entangling Gate for Fixed-Frequency Superconducting Qubits," *Phys. Rev. Lett.*, vol. 107,

- no. 8, p. 80502, Aug. 2011, doi: 10.1103/PhysRevLett.107.080502.
- [5] J. Gambetta, "Quantum-centric supercomputing: a new computational framework for chemistry," in *American Chemical Society (ACS) Spring Meeting*, 2025.
- [6] A. Javadi-Abhari *et al.*, "Quantum computing with Qiskit," pp. 1–19, 2024, [Online]. Available: http://arxiv.org/abs/2405.08810
- [7] "IBM and PINQ<sup>2</sup> unveil utility-scale quantum computer in Québec." [Online]. Available: https://research.ibm.com/blog/ibm-pinq2-quantum-computer-install
- [8] "IBM Quantum." [Online]. Available: https://quantum.ibm.com/
- [9] R. P. Feynman, "Simulating Physics with Computers," vol. 21, pp. 467–488, 1982.

- [10] D. Deutsch, "Quantum Theory, the Church-Turing Principle and the Universal Quantum Computer," *Proc. R. Soc. Lond. A. Math. Phys. Sci.*, vol. 400, no. No. 1818(Jul. 8, 1985), pp. 97–117, 1985.
- [11] E. Bernstein and U. Vaziranit, "Quantum complexity theory," *Proc. Annu. ACM Symp. Theory Comput.*, vol. Part F1295, pp. 11–20, 1993, doi: 10.1145/167088.167097.
- [12] D. Deutsch and R. Jozsa, "Rapid solution of problems by quantum computation," *Proc. R. Soc. London. Ser. A Math. Phys. Sci.*, vol. 439, no. 1907, pp. 553–558, 1992.
- [13] P. W. Shor, T. B. Labs, M. Ave, and M. Hill, "Algorithms for Quantum Computation: Discrete Log and Factoring," *Proc. 35th Annu. Symp. Found. Comput. Sci.*, p. 124, 1994.
- [14] L. K. Grover, "A fast quantum mechanical algorithm for database search," *Proc. Annu. ACM Symp. Theory Comput.*, vol. Part F1294, pp. 212–219, 1996, doi: 10.1145/237814.237866.
- [15] D. R. Simon, "On the power of quantum computation," *SIAM J. Comput.*, vol. 26, no. 5, pp. 1474–1483, 1997, doi: 10.1137/S0097539796298637.
- [16] C. Godfrin *et al.*, "Operating Quantum States in Single Magnetic Molecules: Implementation of Grover's Quantum Algorithm," vol. 187702, no. November, pp. 1–5, 2017, doi: 10.1103/PhysRevLett.119.187702.
- [17] Y. Nakamura, Y. A. Pashkin, and J. S. Tsai, "Coherent control of macroscopic quantum states in a single-Cooper-pair box," *Nature*, vol. 398, no. 6730, pp. 786–788, 1999, doi: 10.1038/19718.
- [18] J. P. Qubit and C. H. Van Der, "Josephson Persistent-Current Qubit," 1999.
- [19] M. H. Devoret and R. J. Schoelkopf, "Superconducting circuits for quantum information: An outlook," *Science* (80-. )., vol. 339, no. 6124, pp. 1169–1174, 2013, doi: 10.1126/science.1231930.
- [20] J. M. Chow *et al.*, "Implementing a strand of a scalable fault-tolerant quantum computing fabric," *Nat. Commun.*, vol. 5, pp. 1–9, 2014, doi: 10.1038/ncomms5015.

- [21] M. AbuGhanem, "IBM Quantum Computers: Evolution, Performance, and Future Directions," pp. 1–29, 2024, [Online]. Available: http://arxiv.org/abs/2410.00916
- [22] A. Y. Kitaev, "Quantum measurements and the Abelian Stabilizer Problem," pp. 1–22, 1995, [Online]. Available: http://arxiv.org/abs/quant-ph/9511026
- [23] L. Hales and S. Hallgren, "An improved quantum Fourier transform algorithm and applications," in *Proceedings 41st Annual Symposium on Foundations of Computer Science*, 2000, pp. 515–525. doi: 10.1109/SFCS.2000.892139.
- [24] I. G. Karafyllidis, "Quantum Computer Simulator Based on the Circuit Model of Quantum Computation," vol. 52, no. 8, pp. 1590–1596, 2005.
- [25] S. Kashani, M. Alqasemi, and J. Hammond, "A quantum Fourier transform (QFT) based note detection algorithm," pp. 1–36, 2022, [Online]. Available: http://arxiv.org/abs/2204.11775
- [26] A. Shakeel, "Efficient and scalable quantum walk algorithms via the quantum Fourier transform," *Quantum Inf. Process.*, vol. 19, no. 9, pp. 1–20, 2020, doi: 10.1007/s11128-020-02834-y.
- [27] Y. Jin *et al.*, "Quantum Fourier Transformation Circuits Compilation," *arXiv Prepr. arXiv2312.16114*, 2023.
- [28] E. Bäumer, V. Tripathi, A. Seif, D. Lidar, and D. S. Wang, "Quantum Fourier Transform using Dynamic Circuits," pp. 1–9, 2024, doi: 10.1103/PhysRevLett.133.150602.
- [29] Y. Yuan *et al.*, "An improved QFT-based quantum comparator and extended modular arithmetic using one ancilla qubit," *New J. Phys.*, vol. 25, no. 10, pp. 1–10, 2023, doi: 10.1088/1367-2630/acfd52.
- [30] D. M. Greenberger, M. A. Horne, and A. Zeilinger, "Going Beyond Bell's Theorem," *Bell's Theorem, Quantum Theory and Conceptions of the Universe*, no. 3, pp. 69–72, 1989, doi: 10.1007/978-94-017-0849-4 10.
- [31] D. M. Greenberger, M. A. Horne, A. Shimony, and A. Zeilinger, "Bell's theorem without

- inequalities," *Am. J. Phys.*, vol. 58, no. 12, pp. 1131–1143, Dec. 1990, doi: 10.1119/1.16243.
- [32] E. D'Hondt and P. Panangaden, "The computational power of the W and GHZ states," *Quantum Inf. Comput.*, vol. 6, no. 2, pp. 173–183, 2006, doi: 10.26421/qic6.2-3.
- [33] W. Feng, P. Wang, X. Ding, L. Xu, and X. Q. Li, "Generating and stabilizing the greenberger-hornezeilinger state in circuit QED: Joint measurement, zeno effect, and feedback," *Phys. Rev. A At. Mol. Opt. Phys.*, vol. 83, no. 4, 2011, doi: 10.1103/PhysRevA.83.042313.
- [34] L. S. Bishop *et al.*, "Proposal for generating and detecting multi-qubit GHZ states in circuit QED," *New J. Phys.*, vol. 11, pp. 1–9, 2009, doi: 10.1088/1367-2630/11/7/073040.
- [35] H. Shimizu, W. Roga, D. Elkouss, and M. Takeoka, "Simple loss-tolerant protocol for GHZ-state distribution in a quantum network," pp. 3–14, 2024, doi: 10.1103/PhysRevA.111.022624.
- [36] Z. Bao *et al.*, "Creating and controlling global Greenberger- Horne-Zeilinger entanglement on quantum processors," *Nat. Commun.*, pp. 1–7, 2024, doi: 10.1038/s41467-024-53140-5.
- [37] J. F. Kam, H. Kang, C. D. Hill, G. J. Mooney, and L. C. L. Hollenberg, "Generation and Preservation of Large Entangled States on Physical Quantum Devices," pp. 1–26, 2023, [Online]. Available: http://arxiv.org/abs/2312.15170
- [38] W. Dü, G. Vidal, and J. I. Cirac, "Three qubits can be entangled in two inequivalent ways," *Phys. Rev. A*, vol. 62, pp. 1–12, 2000, [Online]. Available: https://journals.aps.org/pra/pdf/10.1103/PhysRevA.62. 062314
- [39] H. Buhrman, M. Folkertsma, B. Loff, and N. M. P. Neumann, "State preparation by shallow circuits using feed forward," pp. 1–38, 2023, doi: 10.22331/q-2024-12-09-1552.
- [40] L. Yeh, Scaling W State Circuits in the qudit Clifford Hierarchy, vol. 1, no. 1. Association for Computing Machinery, 2023. doi: 10.1145/3594671.3594687.

- [41] R. Heilmann, M. Gräfe, S. Nolte, and A. Szameit, "A novel integrated quantum circuit for high-order W-state generation and its highly precise characterization," *Sci. Bull.*, vol. 60, no. 1, pp. 96–100, 2015, doi: 10.1007/s11434-014-0688-5.
- [42] C. Yesilyurt *et al.*, "Deterministic local doubling of W states," *J. Opt. Soc. Am. B*, vol. 33, no. 11, pp. 2313–2319, 2016, doi: 10.1364/JOSAB.33.002313.
- [43] Y. S. Weinstein, M. A. Pravia, E. M. Fortunato, S. Lloyd, and D. G. Cory, "Implementation of the Quantum Fourier Transform," *Phys. Rev. Lett.*, vol. 86, no. 9, pp. 1889–1891, Feb. 2001, doi: 10.1103/PhysRevLett.86.1889.
- [44] "A 10-Cluster Entanglement Network on IBM's 127-Qubit Quantum Computer Osaka."
- [45] J. J. Vartiainen, A. O. Niskanen, M. Nakahara, and M. M. Salomaa, "Implementing Shor's algorithm on Josephson charge qubits," *Phys. Rev. A*, vol. 70, no. 1, p. 12319, Jul. 2004, doi: 10.1103/PhysRevA.70.012319.
- [46] I. Qiskit, "QFT-Layput." [Online]. Available: https://docs.quantum.ibm.com/api/qiskit/qiskit.circuit. library.QFT
- [47] L. Zhou, S. Wang, S. Choi, H. Pichler, and M. D. Lukin, "Quantum Approximate Optimization Algorithm: Performance, Mechanism, and Implementation on Near-Term Devices," *Phys. Rev. X*, vol. 10, no. 2, p. 21067, 2020, doi: 10.1103/PhysRevX.10.021067.
- [48] A. Perdomo-ortiz, N. Dickson, M. Drewbrook, and G. Rose, "Finding low-energy conformations of lattice protein models by quantum annealing Alejandro," no. November, 2018.
- [49] N. Sachdeva *et al.*, "Quantum optimization using a 127-qubit gate-model IBM quantum computer can outperform quantum annealers for nontrivial binary optimization problems".
- [50] A. Katabarwa *et al.*, "Early Fault-Tolerant Quantum Computing," *Phys. Rev. Appl.*, vol. 10, no. 1, p. 1, 2024, doi: 10.1103/PRXQuantum.5.020101.
- [51] N. Earnest, C. Tornow, D. J. Egger, and C. Gates, "Pulse-efficient circuit transpilation for

- quantum applications on cross-resonance-based hardware," vol. 043088, pp. 1–11, 2021, doi: 10.1103/PhysRevResearch.3.043088.
- [52] I. P. Galanis, I. K. Savvas, A. V. Chernov, and M. A. Butakova, "Reliability Testing, Noise And Error Correction Of Real Quantum Computing Devices," *Telfor J.*, vol. 13, no. 1, pp. 41–46, 2021, doi: 10.5937/telfor2101041g.
- [53] S. M.-L. Pfaendler, K. Konson, and F. Greinert, "Advancements in Quantum Computing—Viewpoint: Building Adoption and Competency in Industry," *Datenbank-Spektrum*, vol. 24, no. 1, pp. 5–20, 2024, doi: 10.1007/s13222-024-00467-4.
- [54] J. R. Wootton, "Benchmarking near-term devices with quantum error correction," *Quantum Sci. Technol.*, vol. 5, no. 4, 2020, doi: 10.1088/2058-9565/aba038.
- [55] A. D. Córcoles *et al.*, "Demonstration of a quantum error detection code using a square lattice of four superconducting qubits," *Nat. Commun.*, vol. 6, 2015, doi: 10.1038/ncomms7979.
- [56] H. Biswas, "Sensor Signal Malicious Data Binary Classification: A Comparison of QNN, and VQC," in 2024 IEEE Pune Section International Conference (PuneCon), 2024, pp. 1–6. doi: 10.1109/PuneCon63413.2024.10894827.
- [57] H. Biswas, "Data Encoding for VQC in Qiskit, A Comparison With Novel Hybrid Encoding".